

# Broad-Range Modulation of Light Emission in Two-Dimensional Semiconductors by Molecular Physisorption Gating

Sefaattin Tongay,<sup>†,¶</sup> Jian Zhou,<sup>†,¶</sup> Can Ataca,<sup>‡</sup> Jonathan Liu,<sup>†</sup> Jeong Seuk Kang,<sup>†</sup> Tyler S. Matthews,<sup>†</sup> Long You,<sup>§</sup> Jingbo Li,<sup>||</sup> Jeffrey C. Grossman,<sup>‡</sup> and Junqiao Wu<sup>\*,†,⊥</sup>

<sup>†</sup>Department of Materials Science and Engineering, University of California, Berkeley, California 94720, United States

<sup>‡</sup>Department of Materials Science and Engineering, Massachusetts Institute of Technology, Cambridge, Massachusetts 02139, United States

<sup>§</sup>Department of Electrical Engineering and Computer Sciences, University of California, Berkeley, California 94720, United States

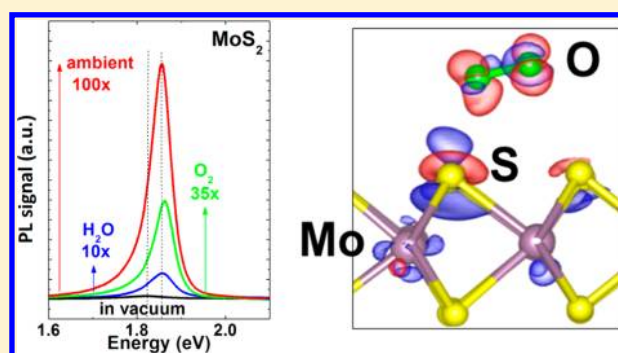
<sup>||</sup>Institute of Semiconductors, Chinese Academy of Sciences, P.O. Box 912, Beijing 100083, People's Republic of China

<sup>⊥</sup>Materials Sciences Division, Lawrence Berkeley National Laboratory, Berkeley, California 94720, United States

## Supporting Information

**ABSTRACT:** In the monolayer limit, transition metal dichalcogenides become direct-bandgap, light-emitting semiconductors. The quantum yield of light emission is low and extremely sensitive to the substrate used, while the underlying physics remains elusive. In this work, we report over 100 times modulation of light emission efficiency of these two-dimensional semiconductors by physical adsorption of O<sub>2</sub> and/or H<sub>2</sub>O molecules, while inert gases do not cause such effect. The O<sub>2</sub> and/or H<sub>2</sub>O pressure acts quantitatively as an instantaneously reversible “molecular gating” force, providing orders of magnitude broader control of carrier density and light emission than conventional electric field gating. Physisorbed O<sub>2</sub> and/or H<sub>2</sub>O molecules electronically deplete n-type materials such as MoS<sub>2</sub> and MoSe<sub>2</sub>, which weakens electrostatic screening that would otherwise destabilize excitons, leading to the drastic enhancement in photoluminescence. In p-type materials such as WSe<sub>2</sub>, the molecular physisorption results in the opposite effect. Unique and universal in two-dimensional semiconductors, the effect offers a new mechanism for modulating electronic interactions and implementing optical devices.

**KEYWORDS:** 2D semiconductors, optical emission, charge transfer, excitons, molecular physisorption



of PL intensity in monolayer TMDs by exposing the sample to O<sub>2</sub> and/or H<sub>2</sub>O gas. The modulation is completely, quantitatively reversible at room temperature by simply controlling the gas pressure, indicating that physisorption of the gas molecules is responsible for the modulation. Inert gases such as Ar and N<sub>2</sub> do not affect the PL intensity. Density functional theory (DFT) calculations discover that the O<sub>2</sub> and H<sub>2</sub>O molecules interact weakly to the TMD monolayers with binding energies ranging from 70 to 140 meV and withdraw a substantial number of electrons from the latter. The charge transfer depletes n-type TMDs (MoS<sub>2</sub> and MoSe<sub>2</sub>) and stabilizes excitons that would be otherwise screened; consequently a new radiative recombination channel is activated, resulting in a remarkable enhancement in the PL intensity. In contrast, the O<sub>2</sub> and H<sub>2</sub>O molecules accumulate the majority holes in p-type TMDs (WSe<sub>2</sub>), resulting in strong

Layered transition metal dichalcogenides (TMDs) with the chemical formula MX<sub>2</sub> (M = Mo, W, Ru and X = S, Se, and Te) display a wide range of attractive physical and chemical properties<sup>1–5</sup> and are potentially important for device applications.<sup>6</sup> Several semiconducting MX<sub>2</sub> show an indirect-to-direct bandgap transition going from the bulk to monolayer. For instance, monolayers of MoS<sub>2</sub>,<sup>1</sup> MoSe<sub>2</sub>,<sup>7</sup> WS<sub>2</sub>,<sup>8,9</sup> and WSe<sub>2</sub><sup>8,9</sup> have direct bandgaps ranging from 1.5 to 2.0 eV. Unusual physical effects, such as valley-selective electronics<sup>3–5</sup> and charged exciton stabilization,<sup>10,11</sup> have been recently observed in monolayer TMDs. Considering the wide range of direct bandgap values available, semiconducting MX<sub>2</sub> in the monolayer limit are especially promising for two-dimensional (2D) optoelectronics, such as light-emitting diodes and optical energy conversion devices.

However, the PL quantum yield of monolayer MX<sub>2</sub> has been found to be low in monolayers.<sup>2</sup> The light-emitting efficiency of these monolayers is highly susceptible to boundary conditions such as the substrate in which they are placed.<sup>2,4</sup> In this work, we demonstrate an unprecedentedly wide range of modulation

of PL intensity in monolayer TMDs by exposing the sample to O<sub>2</sub> and/or H<sub>2</sub>O gas. The modulation is completely, quantitatively reversible at room temperature by simply controlling the gas pressure, indicating that physisorption of the gas molecules is responsible for the modulation. Inert gases such as Ar and N<sub>2</sub> do not affect the PL intensity. Density functional theory (DFT) calculations discover that the O<sub>2</sub> and H<sub>2</sub>O molecules interact weakly to the TMD monolayers with binding energies ranging from 70 to 140 meV and withdraw a substantial number of electrons from the latter. The charge transfer depletes n-type TMDs (MoS<sub>2</sub> and MoSe<sub>2</sub>) and stabilizes excitons that would be otherwise screened; consequently a new radiative recombination channel is activated, resulting in a remarkable enhancement in the PL intensity. In contrast, the O<sub>2</sub> and H<sub>2</sub>O molecules accumulate the majority holes in p-type TMDs (WSe<sub>2</sub>), resulting in strong

Received: March 27, 2013

Revised: April 25, 2013

Published: April 29, 2013

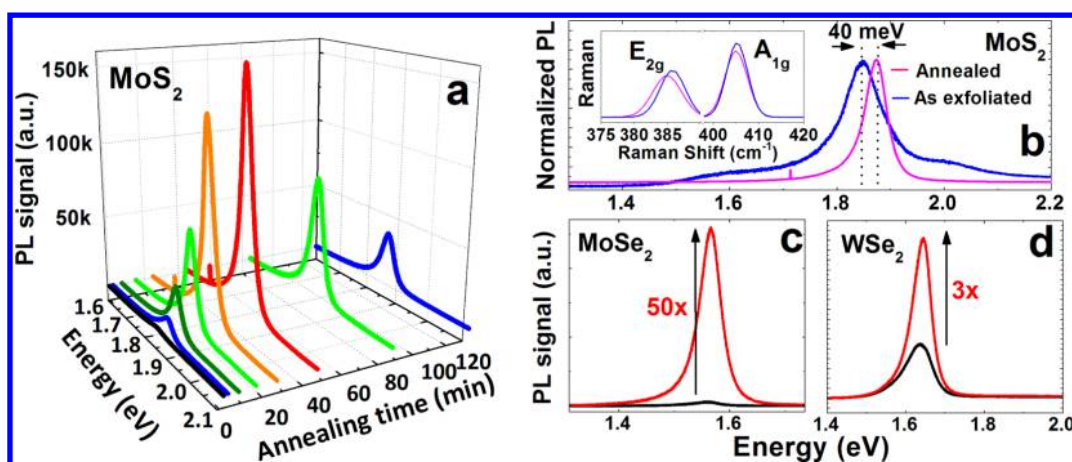


**Figure 1.** Drastic enhancement in room-temperature photoluminescence intensity of monolayer TMDs by thermal annealing. (a) PL spectrum of monolayer MoS<sub>2</sub> as a function of annealing time. The anneal is at 450 °C in vacuum. The laser excitation intensity is fixed at  $4 \times 10^4$  W/m<sup>2</sup> for the PL measurements. (b) Normalized PL spectrum for pristine and optimally annealed monolayer MoS<sub>2</sub>. (Inset) Raman spectrum of pristine and annealed monolayer MoS<sub>2</sub>. (c) PL intensity enhancement of monolayer MoSe<sub>2</sub> upon thermal anneal at 250 °C for 15 min. The peak is blue shifted by  $\sim 17$  meV. (d) PL intensity enhancement of monolayer WSe<sub>2</sub> upon thermal anneal at 300 °C for 10 min. The peak shift is blue shifted by  $\sim 10$  meV. All the PL measurements are taken at room temperature in ambient condition.

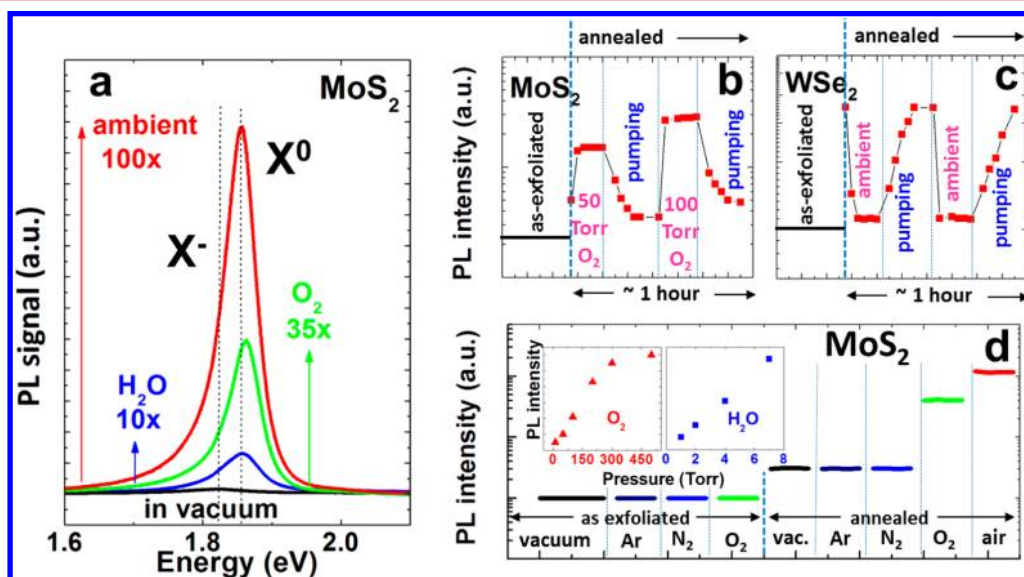


**Figure 2.** Effects of exposure to different gas species on the PL intensity of annealed monolayer TMDs. (a) Change in PL of MoS<sub>2</sub> (from its annealed but measured in vacuum value) upon exposure to H<sub>2</sub>O alone, O<sub>2</sub> alone, and ambient air. The pressure of these gases is 7, 200, and 760 Torr, respectively. Trion X<sup>-</sup> and exciton X<sup>0</sup> peak positions are indicated. (b) Modulation of the PL intensity of monolayer MoS<sub>2</sub> as a function of O<sub>2</sub> purging (50 and 100 Torr, respectively) and pumping. (c) Modulation of the PL intensity of monolayer WSe<sub>2</sub> as a function of ambient air purging (760 Torr) and pumping. Note the opposite response in MoS<sub>2</sub> and WSe<sub>2</sub>. The time periods of purging and pumping in panels b and c are on the order of minutes. (d) Effect of Ar, N<sub>2</sub>, O<sub>2</sub>, and air on the PL intensity of annealed and as-exfoliated monolayer MoS<sub>2</sub>. Inset: PL intensity as a function of O<sub>2</sub> and H<sub>2</sub>O pressure. Note the log scale of PL intensity in panels b, c, and d.

suppression of the PL. In addition to the PL intensity modulation, the PL peak position also slightly shifts, which is explained by a switch between neutral exciton recombination and charged exciton (trion) recombination. The molecular physisorption, acting as a gating force, provides much wider control of charge density and light emission than conventional electric field gating and is free of limitations in the latter that are imposed by dielectric breakdown, metal contacts, and device fabrication. Such results and understanding not only shed new light on many-body physics in 2D semiconductors but also provides a foundation for new optoelectronic devices where strong PL modulation by external means is desired.

**Annealing and Molecular Physisorption Effects.** The TMD flakes were mechanically exfoliated from bulk crystals (see Methods) onto 90 nm thick thermal silicon oxide where a relatively high contrast can be observed for the flakes.<sup>12</sup> Monolayer TMD typically displays a thickness of  $\sim 0.7$  nm as determined by atomic force microscopy (AFM). The monolayers could also be identified by other complementary methods such as microscale Raman spectroscopy and PL measurements (see Supporting Information). From bulk to monolayers, the out-of-plane Raman mode (A<sub>1g</sub>) softens while the in-plane mode (E<sub>2g</sub>) stiffens.<sup>13</sup> Consistent with previous reports,<sup>1,2</sup> stronger PL is observed from monolayer TMDs compared to its multilayer and bulk counterparts. At room

temperature, monolayer MoS<sub>2</sub>, MoSe<sub>2</sub>, and WSe<sub>2</sub> show a prominent PL peak at ~1.84, 1.56, and 1.63 eV, respectively.

To attain the sensitivity to gas molecules, an anneal-based “forming process” is needed for as-exfoliated TMD monolayers. Here, the forming process can be pictured as a process to expose the monolayer surface to the ambient by thermally driving away contaminants/organic residue, which is similar to the sample preparation techniques commonly used for scanning tunneling microscopy or releasing stress built in the monolayers by the substrate. Another possibility is that the forming process might be creating a small density of chalcogen vacancies in the monolayer (Figure S3 in Supporting Information). Figure 1a shows PL spectrum of a monolayer MoS<sub>2</sub> measured at room temperature after 450 °C anneal in vacuum for different annealing times. A 40 min anneal at 450 °C enhances the PL intensity by over 50 times, while the full width at half-maximum (fwhm) of the PL peak decreases from 90 to 45 meV, and the PL peak position shifts from ~1.84 to ~1.88 eV, as shown in the normalized PL plot (Figure 1b). A comparison between the Raman spectrum of pristine (i.e., as-exfoliated) and optimally annealed monolayer MoS<sub>2</sub> (Figure 1b inset) shows that the fwhm and peak intensity of the A<sub>1g</sub> and E<sub>2g</sub> peaks remain largely unchanged, therefore the thermal anneal does not degrade the crystalline quality of the material. However, the in-plane Raman mode (E<sub>2g</sub>) softens from 384.5 to 383 cm<sup>-1</sup>, possibly attributed to desorption of contamination molecules and/or releasing stress on the monolayers. This change is irreversible; that is, subsequent treatments (further annealing and pumping/purging of gas) do not cause further changes to the Raman spectrum. We found that 40 min anneal at 450 °C optimally enhances the PL intensity. The enhancement is less for both weaker (shorter times or lower temperatures) and stronger annealing (longer times or higher temperatures). This is a general effect, as other 2D semiconductors, monolayer MoSe<sub>2</sub> and WSe<sub>2</sub> (Figure 1c,d), also exhibits similar behavior but with different optimal annealing condition.

After the forming process, the photoluminescence intensity of monolayer TMDs becomes extremely sensitive to gas environment. In the following discussion, we first focus on MoS<sub>2</sub>. Immediately after annealing, the MoS<sub>2</sub> was transferred into a vacuum chamber for micro-PL measurements. The chamber was pumped down to 10<sup>-4</sup> Torr prior to backfilling with different gases at controlled pressures. As shown in Figure 2a, upon exposing the MoS<sub>2</sub> to H<sub>2</sub>O alone (7 Torr), O<sub>2</sub> alone (200 Torr), or O<sub>2</sub> and H<sub>2</sub>O together, the PL intensity was enhanced by 10, 35, and 100 times, respectively. When the gas pressure changes, the PL intensity also changes instantaneously, and the time it takes for the MoS<sub>2</sub> to reach the new PL intensity is merely limited by the pumping/purging speed and the time needed for the PL measurement, as shown in Figure 2b. The PL remains constant over a time frame of days, as long as the gas pressure stays constant. Pumping the O<sub>2</sub> or H<sub>2</sub>O gas out of the chamber, the PL intensity immediately reverts back to its original value (i.e., postanneal PL measured in vacuum), implying that the O<sub>2</sub> and H<sub>2</sub>O molecules are physisorbed, as opposed to chemisorbed, on the MoS<sub>2</sub> surface. The PL can be reversibly modulated for numerous times by pumping and purging with O<sub>2</sub> and/or H<sub>2</sub>O. The PL intensity is nearly linearly proportional to the O<sub>2</sub> or H<sub>2</sub>O pressure, as shown in the inset of Figure 2d. This is consistent with the physisorption picture of molecules, because in equilibrium sheet density of physisorbed molecules on the surface is proportional to the gas pressure. Above a particular O<sub>2</sub> pressure (Figure 2d inset), the

PL intensity displays a tendency to saturate. This threshold value depends possibly on the average distance between the physisorbed O<sub>2</sub> molecules, which determines the largest effective area where O<sub>2</sub> can interact with the MoS<sub>2</sub>. For the H<sub>2</sub>O experiment, the pressure cannot be increased more than 7 Torr due to instrumental limitations, and in the 0–7 Torr range such saturation in PL enhancement was not observed. Exposing the annealed MoS<sub>2</sub> to inert gases of Ar or N<sub>2</sub> does not change its PL intensity (Figure 2d); therefore, the PL enhancement must be attributed to the molecular property of O<sub>2</sub> and H<sub>2</sub>O interacting with MoS<sub>2</sub>. We also note that when both O<sub>2</sub> and H<sub>2</sub>O interacts with MoS<sub>2</sub> (in ambient air), the PL enhancement surpasses that of O<sub>2</sub> or H<sub>2</sub>O alone, as the different types of gas molecules simultaneously deplete the monolayer. More interestingly, while MoSe<sub>2</sub> exhibits similar gas sensitivity (not shown here) as MoS<sub>2</sub>, WSe<sub>2</sub> shows the opposite behavior (Figure 2c); that is, exposing to O<sub>2</sub> and/or H<sub>2</sub>O strongly suppresses the PL of monolayer WSe<sub>2</sub>.

**Density Functional Theory Calculations.** To provide a physical picture for the effect of O<sub>2</sub> and H<sub>2</sub>O, we simulated the interaction between monolayer MoS<sub>2</sub> and O<sub>2</sub> or H<sub>2</sub>O molecules using density functional theory (DFT) calculations. Calculating the van der Waals energy between the molecule and MoS<sub>2</sub> as a function of angle and distance reveals that O<sub>2</sub> and H<sub>2</sub>O molecules can be physisorbed on the MoS<sub>2</sub> surface with 79 and 110 meV binding energies, respectively. Once physisorbed, the O<sub>2</sub> or H<sub>2</sub>O molecule is blocked from chemisorption by a high energy barrier (~2 eV), but approximately 0.04 electrons per O<sub>2</sub> and 0.01 electrons per H<sub>2</sub>O are transferred to the molecules, depleting the monolayer MoS<sub>2</sub>, as shown in Figure 3a,b. Because of the monolayer thickness of the MoS<sub>2</sub>, the total number of charge transferred from the MoS<sub>2</sub> to the gas molecules adds up to remarkably high

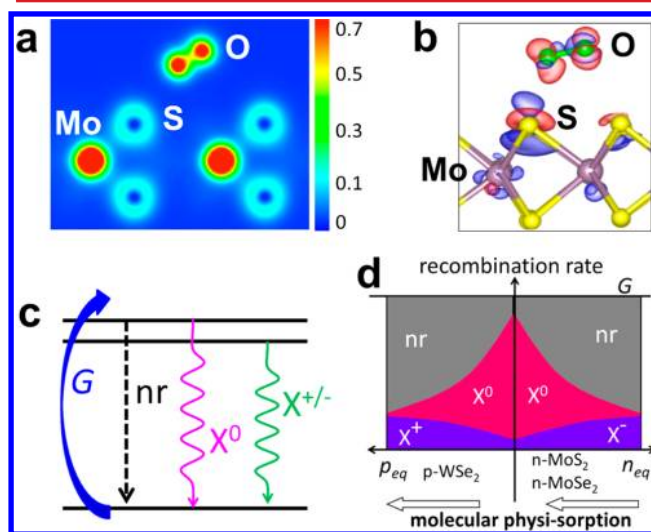


**Figure 3.** Recombination and charge transfer under physisorbed O<sub>2</sub> or H<sub>2</sub>O. (a) Charge density distribution of an O<sub>2</sub> molecule physisorbed on the MoS<sub>2</sub> surface. The color scale is in the units of e/Å<sup>3</sup>. (b) Charge density difference between pristine MoS<sub>2</sub> and O<sub>2</sub>-adsorbed MoS<sub>2</sub>. The iso-surface is for electron density of 2 × 10<sup>-4</sup> e/Å<sup>3</sup>. Red is charge accumulation and blue is charge depletion. (c) Schematic of the excitation and recombination process. The nonradiative recombination, exciton recombination, and trion recombination are represented by the process of nr, X<sup>0</sup>, and X<sup>-</sup>, respectively. (d) Rate of nr, X<sup>0</sup>, and X<sup>-</sup> (or X<sup>+</sup>) as a function of equilibrium electron density in n- (or p-) type 2D semiconductors.

sheet densities. Assuming that one O<sub>2</sub> molecule is physisorbed on each unit cell of MoS<sub>2</sub>, the charge transfer would reduce the original sheet carrier density as much as  $5 \times 10^{13}/\text{cm}^2$ . This number can reach even higher values if the physisorption occurs at defect sites where the charge transfer is higher. For example, we find that the O<sub>2</sub> and H<sub>2</sub>O molecules bind more strongly at sulfur-vacancy sites (110 meV for O<sub>2</sub> and 150 meV for H<sub>2</sub>O), and for H<sub>2</sub>O the charge transfer per molecules increases by a factor of 5.

**Discussion.** The observations in Figures 1 and 2 can be summarized as a drastic enhancement in PL intensity accompanied with a peak shift from 1.84 to 1.88 eV when the monolayer MoS<sub>2</sub> is electrically depleted of free electrons. Compared with literature data,<sup>10</sup> the high-energy peak at  $\sim 1.88$  eV is associated with recombination of neutral excitons (X<sup>0</sup>), while the low-energy peak at 1.84 eV with negatively charged excitons (trion, X<sup>-</sup>), that is, an electron bound to a neutral exciton. The energy difference of  $\sim 40$  meV is attributed to the binding energy ( $E_{b1}$ ) of the second electron in X<sup>-</sup>. It has been predicted that due to a higher  $E_{b1}$ , it is much easier to observe radiative recombination of trions in quantum confined systems.<sup>14</sup> Values of  $E_{b1}$  ranging from 2 to 6 meV were reported for semiconductor quantum dots and quantum wells at temperatures typically below 10 K.<sup>15–19</sup> It was recently reported to be  $\sim 40$  meV for ungated monolayer MoS<sub>2</sub> at 14K,<sup>4,10</sup> and 30 meV for monolayer MoSe<sub>2</sub> at 20K.<sup>11</sup> In those experiments, the relative PL intensities of X<sup>-</sup> and X<sup>0</sup> could be slightly tuned by electrostatically controlling the charge state of the material.

The as-exfoliated MoS<sub>2</sub> is known to be unintentionally n-type doped<sup>4,6,10</sup> with a high sheet density of equilibrium electrons ( $n_{\text{eq}}$ ) up to  $10^{13}/\text{cm}^2$ . The rate equation of nonequilibrium free electrons ( $n$ ) under photoexcitation and recombination is

$$\frac{dn}{dt} = G - \frac{n \cdot \eta_{X^0}}{\tau_{\text{nr}}} - \frac{n \cdot \eta_{X^0}}{\tau_{X^0}} - \frac{n \cdot \eta_{X^-}}{\tau_{X^-}} \quad (1)$$

where  $G$  is the photoexcitation rate, and the subscription “nr”, “X<sup>0</sup>” and “X<sup>-</sup>” stands for nonradiative (including defects-mediated and Auger process), neutral exciton radiative, and trion radiative recombination process, respectively.  $\tau$  is recombination lifetime;  $\eta$  is the probability of an electron falling into one of these three pathways (Figure 3c), which satisfies  $\eta_{\text{nr}} + \eta_{X^0} + \eta_{X^-}$ . In the presence of high  $n_{\text{eq}}$ , the probability of forming X<sup>0</sup> and X<sup>-</sup> (i.e.,  $\eta_{X^0}$  and  $\eta_{X^-}$ ) is expected to rapidly decrease due to electrostatic screening between free electrons and holes,<sup>18</sup> on the other hand, high  $n_{\text{eq}}$  favors formation of X<sup>-</sup> (but not X<sup>0</sup>) by providing the second electron for trions. As a result,  $\eta_{X^-}$  and  $\eta_{X^0}$  have very different functional dependence on  $n$  and  $n_{\text{eq}}$ . In steady state, the  $n_{\text{eq}}$  dependence of the rate of nonradiative recombination, exciton radiative, and trion radiative recombination is schematically shown in Figure 3d. It can be seen that for as-exfoliated monolayer MoS<sub>2</sub> where  $n_{\text{eq}}$  is high, X<sup>0</sup> is destabilized due to charge screening while X<sup>-</sup> recombination is relatively high due to the abundance of free electrons. The total radiation intensity is low, because most photoexcited electrons and holes are forced to recombine nonradiatively; The nonradiative recombination may be dominated by the Auger process at such high  $n_{\text{eq}}$ . As the monolayer MoS<sub>2</sub> physisorbs electronegative molecules such as O<sub>2</sub> and H<sub>2</sub>O,  $n_{\text{eq}}$  is much depleted by the charge transfer. Consequently, X<sup>0</sup> is stabilized while X<sup>-</sup> is depleted, resulting in a high intensity of X<sup>0</sup> and a diminishing X<sup>-</sup> peak in the PL

spectrum. Therefore, the modulation of PL between the X<sup>0</sup> peak at 1.88 eV and X<sup>-</sup> peak at 1.84 eV is a direct result of competition between charge screening that destabilizes both excitons and trions, and charge accumulation that is needed for trions but not for excitons. We note that the tail at the low-energy shoulder of the X<sup>0</sup> PL peaks in Figure 2a is probably caused by disorder and defects, as is in conventional semiconductors. It is not attributed to a residual X<sup>-</sup> signal, which is overshadowed by the much stronger X<sup>0</sup>.

The behavior of recombination rates in Figure 3d is consistent with the recent report by Mak et al.<sup>10</sup> that at low temperature the X<sup>0</sup> emission intensity is gate voltage dependent, while that of X<sup>-</sup> is mostly gate voltage independent. It is not surprising that electric field gating (in vacuum) has a much weaker effect on the PL intensity than molecular physisorption, because the modulation range of sheet carrier density by gate field is typically well below  $10^{13}/\text{cm}^2$ , limited by breakdown of the gating dielectric. The reversible physisorption acts as a kind of “molecular gating” to withdraw a large density of electrons and drastically modulate the PL. At subatmosphere gas pressures, the molecular gating can easily modulate the sheet carrier density much beyond the dielectric breakdown point that limits conventional electric field gating.

The understanding can be generalized to other monolayer TMDs. We find that after the anneal-forming process, MoSe<sub>2</sub> behaves very similarly to MoS<sub>2</sub> in the interaction with O<sub>2</sub>/H<sub>2</sub>O, while WSe<sub>2</sub> shows the opposite behavior (Figure 2c). The PL intensity of WSe<sub>2</sub> is the highest when measured in vacuum and suppressed by the presence of O<sub>2</sub> and/or H<sub>2</sub>O. This is understood considering that as-exfoliated WSe<sub>2</sub> is p-type,<sup>20</sup> while MoS<sub>2</sub> and MoSe<sub>2</sub> are both n-type. The different types of native doping are related to the high-lying valence band maximum of WSe<sub>2</sub> and low-lying conduction band minimum of MoS<sub>2</sub> and MoSe<sub>2</sub>.<sup>21</sup> Therefore, the electron transfer to O<sub>2</sub> or H<sub>2</sub>O molecules depletes the majority (electrons,  $n_{\text{eq}}$ ) in MoS<sub>2</sub> and MoSe<sub>2</sub> but accumulates the majority (holes,  $p_{\text{eq}}$ ) in WSe<sub>2</sub>. As a result, the PL intensity of X<sup>0</sup> is reduced by physisorption of O<sub>2</sub>/H<sub>2</sub>O in WSe<sub>2</sub>, as shown schematically in Figure 3d. The PL peak shift in Figure 1c,d gives a room-temperature binding energy of negative trion X<sup>-</sup>  $\sim 17$  meV in MoSe<sub>2</sub>, and of positive trion X<sup>+</sup>  $\sim 10$  meV in WSe<sub>2</sub>.

Lastly, we emphasize that the charge transfer between the gas molecules and the monolayer MX<sub>2</sub> is the most important factor in PL modulation. The annealing is only a necessary prestep to activate the molecule adsorption. The reported PL modulation might be enhanced even more by activating N<sub>2</sub> molecules in air, so that they also transfer charges with the monolayer, as O<sub>2</sub> molecules do. One way to achieve this is to intentionally create point defects in the monolayer, where the electronic interaction with N<sub>2</sub> molecules is artificially activated. It is also possible to enhance the charge transfer by modifying the MX<sub>2</sub> surface with chemical agents that sensitize the surface to gas molecules.

**Conclusions.** In summary, we have shown a universal effect that the light emission efficiency in 2D semiconductors is dominated by charge transfer to physically adsorbed electronegative gas molecules such as O<sub>2</sub> and H<sub>2</sub>O. The process is unique in such 2D system not only because of its high surface area that is prone to interactions with gaseous molecules, but also its 2D nature that stabilizes many-body exciton effects. The effect not only enables reversible, quantitative control of light emission intensity with gas pressure as a gating force, a desired function for new applications such as sensors, phosphors, and optical switch, but also highlights the importance of interaction

with gases/ambient air that greatly affects the optical properties of monolayer TMDs.

**Methods.** *Sample Preparation and Micro-PL/Raman Measurements.* Monolayer MoX<sub>2</sub> flakes were exfoliated from bulk crystals (2D semiconductors and SPI) onto p-type Si wafer (MTI corporation, resistivity 0.001–0.1 Ωcm) with 90 nm thermal oxide. Measurements were performed using a Renishaw micro-PL/Raman system. The laser beam (wavelength 488 nm) was focused onto the sample (spot diameter of ~1–2 μm) using excitation power up to 2–5 μW. The PL/Raman measurements in different gas conditions were performed in a homemade vacuum chamber pumped down to ~10<sup>-4</sup> Torr using a turbo-molecular pump. O<sub>2</sub>, Ar, or N<sub>2</sub> gas was introduced into the chamber regulated by flow meters and the pressure was measured by a vacuum gauge. The effect of H<sub>2</sub>O was tested by electrically heating up a quartz crucible of deionized water near the sample to create a H<sub>2</sub>O-rich environment.

**Thermal Annealing.** The samples were heated to 450 °C in a 30 °C/min rate and the temperature was held at 450 ± 0.1 °C for different duration times. The annealing was performed in a 2 in. quartz tube in vacuum (30 mTorr base pressure). Prior to the annealing, the quartz tube was cleaned at 1000 °C in H<sub>2</sub> gas (2 Torr) for a couple hours. After annealing, the furnace was cooled down to room temperature at a fast rate and the samples were taken out of the furnace and immediately transferred to the Raman chamber for optical measurements.

**Density Functional Theory Calculations.** Our calculations were based on first-principles DFT using projector-augmented wave potentials.<sup>22</sup> The exchange correlation potential has been represented by the generalized gradient approximation characterized by Perdew–Burke–Ernzerhof<sup>23</sup> including van der Waals corrections<sup>24</sup> both for spin-polarized and spin-unpolarized cases. Effects of spin–orbit coupling and noncollinear magnetism were taken into account in the spin-polarized calculations. The supercell size, kinetic energy cutoff, and Brillouin zone sampling of the calculations were determined after extensive convergence analyses. A large spacing of ~15 Å between the 2D single layers was used to prevent interlayer interactions. A plane-wave basis set with kinetic energy cutoff of 300 eV was used. In the self-consistent field potential and total energy calculations, the Brillouin zone was sampled by special *k*-points. The numbers of these *k*-points were (25 × 25 × 1) and (15 × 15 × 5) for the primitive 1H-MoS<sub>2</sub> and were scaled according to the size of the super cells. All atomic positions and lattice constants were optimized using the conjugate gradient method, where the total energy and atomic forces were minimized. The convergence for energy were chosen to be 10<sup>-6</sup> eV between two consecutive steps, and the maximum Hellmann–Feynman forces acting on each atom was less than 0.01 eV/Å upon ionic relaxation. The pressure in the unit cell was kept below 5 kbar. Numerical calculations were performed by using the VASP software.<sup>25</sup>

## ■ ASSOCIATED CONTENT

### 📄 Supporting Information

Experimental specifics, materials preparation including MoS<sub>2</sub>, MoSe<sub>2</sub>, and WSe<sub>2</sub>, and Supporting Information on annealing effects. This material is available free of charge via the Internet at <http://pubs.acs.org>.

## ■ AUTHOR INFORMATION

### Corresponding Author

\*E-mail: [wuj@berkeley.edu](mailto:wuj@berkeley.edu).

### Author Contributions

¶S.T. and J.Z. contributed equally

### Notes

The authors declare no competing financial interest.

## ■ ACKNOWLEDGMENTS

This work was supported by the U.S. Department of Energy Early Career Award DE-FG02-11ER46796. Part of the materials processing and device fabrication used facilities at the Lawrence Berkeley National Laboratory, which is supported by the Office of Science, Office of Basic Energy Sciences, of the U.S. Department of Energy under Contract No. DE-AC02-05CH11231. We thank Dr. Changyun Ko for his help on nano-Auger measurements.

## ■ REFERENCES

- (1) Splendiani, A.; Sun, L.; Zhang, Y.; Li, T.; Kim, J.; Chim, C. Y.; Galli, G.; Wang, F. Emerging Photoluminescence in Monolayer MoS<sub>2</sub>. *Nano Lett.* **2010**, *10*, 1271.
- (2) Mak, K.; Lee, C.; Hone, J.; Shan, J.; Heinz, T. F. Atomically Thin MoS<sub>2</sub>: A New Direct-Gap Semiconductor. *Phys. Rev. Lett.* **2010**, *105*, 136805.
- (3) Zeng, H.; Dai, J.; Yao, W.; Xiao, D.; Cui, X. Valley polarization in MoS<sub>2</sub> monolayers by optical pumping. *Nat. Nanotechnol.* **2012**, *7*, 490.
- (4) Mak, K.; He, K.; Shan, J.; Heinz, T. F. Control of valley polarization in monolayer MoS<sub>2</sub> by optical helicity. *Nat. Nanotechnol.* **2012**, *7*, 494.
- (5) Cao, T.; et al. Valley-selective circular dichroism of monolayer molybdenum disulphide. *Nat. Commun.* **2012**, *3*, 887.
- (6) Radisavljevic, B.; Radenovic, A.; Brivio, J.; Giacometti, V.; Kis, A. Single-layer MoS<sub>2</sub> transistors. *Nat. Nanotechnol.* **2012**, *6*, 147.
- (7) Tongay, S.; Zhou, J.; Ataca, C.; Lo, K.; Matthews, T. S.; Li, J.; Grossman, J. C.; Wu, J. Thermally driven crossover from indirect toward direct bandgap in 2D semiconductors: MoSe<sub>2</sub> versus MoS<sub>2</sub>. *Nano Lett.* **2012**, *12*, 5576.
- (8) Ataca, C.; Sahin, H.; Ciraci, S. Stable, Single-Layer MX<sub>2</sub> Transition-Metal Oxides and Dichalcogenides in a Honeycomb-Like Structure. *J. Chem. Phys. C* **2012**, *116*, 8983.
- (9) Yun, W. S.; Han, S. W.; Hong, S. C.; Kim, I. G.; Lee, J. D. Thickness and strain effects on electronic structures of transition metal dichalcogenides: 2H-MX<sub>2</sub> semiconductors (M = Mo, W; X = S, Se, Te). *Phys. Rev. B* **2012**, *85*, 033305.
- (10) Mak, K. F.; He, K.; Lee, C.; Lee, G. H.; Hone, J.; Heinz, T. F.; Shan, J. Tightly bound trions in monolayer MoS<sub>2</sub>. *Nat. Mater.* **2012**, *12*, 207.
- (11) Ross, J.; et al. Electrical Control of Truly Two Dimensional Neutral and Charged Excitons in a Monolayer Semiconductor. *Nat. Commun.* **2012**, *4*, 1474.
- (12) Benameur, M. M.; Radisavljevic, B.; Héron, J. S.; Sahoo, S.; Berger, H.; Kis, A. Visibility of dichalcogenide nanolayers. *Nanotechnology* **2011**, *22*, 125706.
- (13) Lee, C.; Yan, H.; Brus, L. E.; Heinz, T. F.; Hone, J.; Ryu, S. Anomalous Lattice Vibrations of Single- and Few-Layer MoS<sub>2</sub>. *ACS Nano* **2010**, *4*, 2695.
- (14) Stebe, B.; Ainane, A. Ground state energy and optical absorption of excitonic trions in two dimensional semiconductors. *Superlattices Microstruct.* **1989**, *5*, 545.
- (15) Esser, A.; Runge, E.; Zimmermann, R.; Langbein, W. Photoluminescence and radiative lifetime of trions in GaAs quantum wells. *Phys. Rev. B* **2000**, *62*, 8232.
- (16) Kheng, K.; Cox, R. T.; Merle d'Aubigne, Y.; Bassani, F.; Saminadayar, K.; Tatarenko, S. Observation of Negatively Charged

Excitons X in Semiconductor Quantum Wells. *Phys. Rev. Lett.* **1993**, *71*, 1752.

(17) Warburton, R. J.; Schaefflein, C.; Haft, D.; Bickel, F.; Lorke, A.; Karrai, K.; Garcia, J. M.; Schoenfeld, W.; Petroff, P. M. Optical emission from a charge-tunable quantum ring. *Nature* **2000**, *405*, 926.

(18) Finkelstein, G.; Shtrikman, H.; Bar-Joseph, I. Optical Spectroscopy of a Two-Dimensional Electron Gas near the Metal-Insulator Transition. *Phys. Rev. Lett.* **1995**, *74*, 976.

(19) Huard, V.; Cox, R. T.; Saminadayar, K.; Arnoult, A.; Tatarenko, S. Bound States in Optical Absorption of Semiconductor Quantum Wells Containing a Two-Dimensional Electron Gas. *Phys. Rev. Lett.* **2000**, *84*, 187.

(20) Fang, H.; Chuang, S.; Chang, T. C.; Takei, K.; Takahashi, T.; Javey, A. High-Performance Single Layered WSe<sub>2</sub> p-FETs with Chemically Doped Contacts. *Nano Lett.* **2012**, *12*, 3788.

(21) Kang, J.; Tongay, S.; Zhou, J.; Li, J.; Wu, J. Band offsets and Heterostructures of Two-Dimensional Semiconductors. *Appl. Phys. Lett.* **2013**, *102*, 012111.

(22) Blochl, P. E. Projector augmented-wave method. *Phys. Rev. B* **1994**, *50*, 17953.

(23) Perdew, J. P.; Burke, K.; Ernzerhof, M. Generalized Gradient Approximation Made Simple. *Phys. Rev. Lett.* **1996**, *77*, 3865.

(24) Grimme, S. Semiempirical GGA-type density functional constructed with a long-range dispersion correction. *J. Comput. Chem.* **2006**, *27*, 1787.

(25) Kresse, G.; Hafner, J. Ab initio molecular dynamics for liquid metals. *Phys. Rev. B* **1993**, *47*, 558.

## Supporting Information to

# Broad-range modulation of light emission in two-dimensional semiconductors by molecular physi-sorption gating

Sefaattin Tongay, Jian Zhou, Can Ataca, Jonathan Liu, Jeong Seuk Kang, Tyler S. Matthews, Long You, Jingbo Li, Jeffrey C. Grossman and Junqiao Wu

### 1. Material preparation and characterization

The MoS<sub>2</sub> flakes were mechanically exfoliated from bulk crystals of 2H-MoS<sub>2</sub> (supplied from SPI Inc and 2Dsemiconductors.com) onto 90 nm thermal oxide SiO<sub>2</sub> on a Si wafer (MTI corporation) (Fig.S1a and c) [1]. The monolayer nature of the measured MoS<sub>2</sub> flakes was checked by three complementary and non-destructive methods: Atomic force microscopy (AFM), Raman spectroscopy, and photoluminescence. During the PL and Raman measurements, we have used very low power on the samples to avoid local heating or damaging effect. AFM line scans on the monolayer MoS<sub>2</sub> typically resulted in ~ 0.7 nm step height, which is the c-axis lattice constant of monolayer MoS<sub>2</sub>. Raman spectroscopy measurements showed that from bulk to single layers, the out-of-plane mode (A<sub>1g</sub>) softens while in-plane (E<sub>2g</sub>) stiffens, resulting in a ~18 cm<sup>-1</sup> difference between these two peaks (Fig.S1b) [2]. Such frequency difference implies that the flakes are monolayers consistent with previous studies [2]. Similar response in frequency difference was observed for MoSe<sub>2</sub> and WSe<sub>2</sub> flakes as function of number of layers and the Raman spectrum of monolayers are shown in Fig.S1c. Lastly, the micro-PL yielded orders of magnitude larger PL intensity for monolayer MoS<sub>2</sub>, MoSe<sub>2</sub>, and WSe<sub>2</sub> compared to their few-layer / bulk (Fig.S1d), attributed to the crossover from indirect to direct bandgap [3].

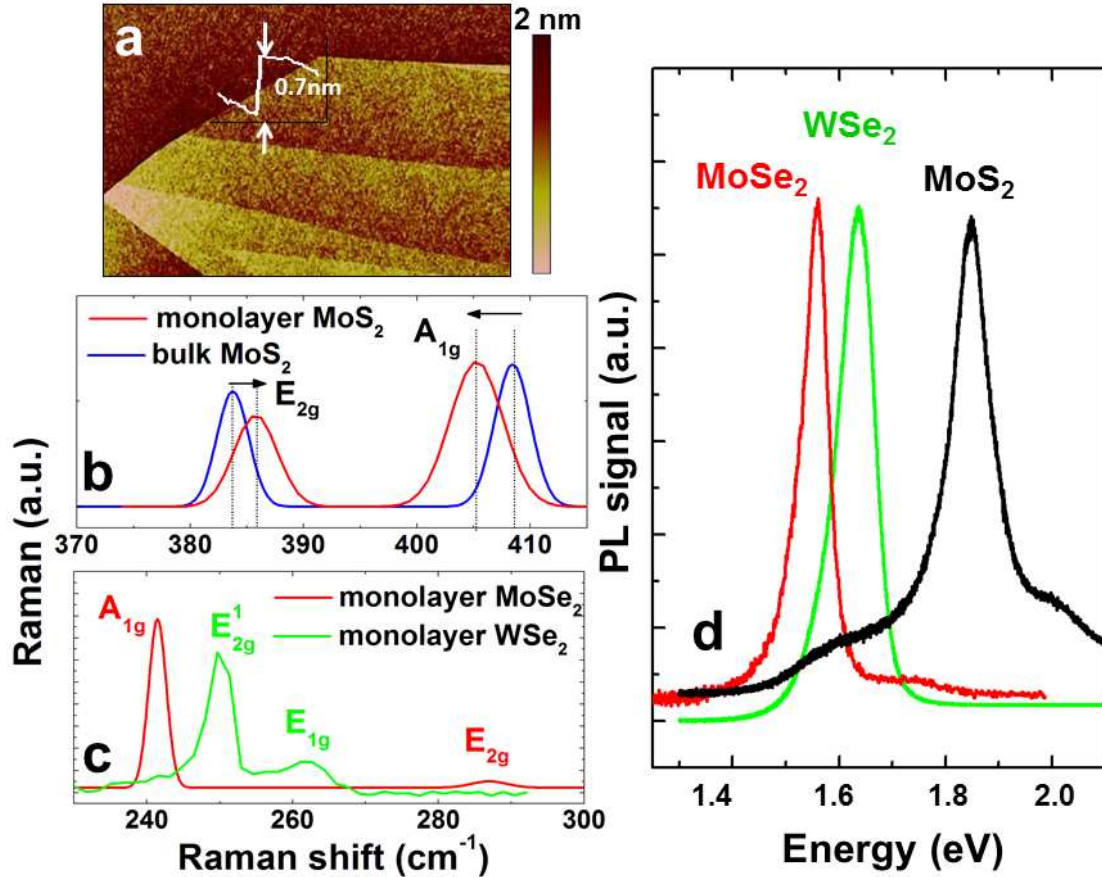


**Figure S1** Characterization of monolayer  $\text{MoS}_2$  exfoliated onto  $90\text{nm SiO}_2$ . **a.** Atomic force microscopy image taken on the  $\text{MoS}_2$  flakes. The monolayer  $\text{MoS}_2$  yields  $0.7\text{nm}$  thickness corresponding to the  $c$ -axis lattice constant of  $1\text{H-MoS}_2$ . **b.** Raman spectrum taken on bulk and monolayer  $\text{MoS}_2$ . **c.** The Raman spectrum of monolayer  $\text{MoSe}_2$  and  $\text{WSe}_2$ . The out-of-plane mode of  $\text{WSe}_2$  is much weaker than the in-plane mode located at around  $180\text{ cm}^{-1}$ . **d.** Normalized photoluminescence (PL) data taken on monolayer  $\text{MoS}_2$ ,  $\text{MoSe}_2$ , and  $\text{WSe}_2$ .

## 2. Effects of annealing

We note that the annealing temperature has a significant impact on the PL enhancement. In Fig.S2, the PL signal is shown for monolayer  $\text{MoS}_2$  annealed in vacuum ( $35\text{mTorr}$  base pressure) at different temperatures ranging from room temperature ( $20^\circ\text{C}$ ) up to  $600^\circ\text{C}$ . Annealing the monolayer  $\text{MoS}_2$  in the  $20\text{-}300^\circ\text{C}$  range followed by exposing to ambient air does not modulate the PL intensity significantly. The monolayer  $\text{MoS}_2$  shows high sensitivity to gas environment after being annealed at  $450^\circ\text{C}$ . Annealing beyond  $550^\circ\text{C}$  resulted in visible decomposition in the flakes and induced large amount of disorder in the system. As a result, photo-excited carriers recombine non-radiatively, and the PL intensity decreases even below the pristine values.



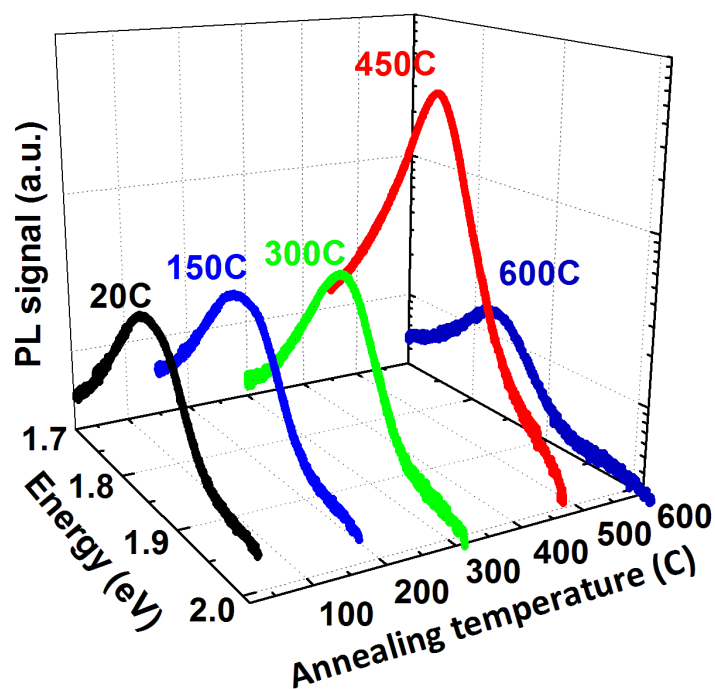


**Figure S2.** Change in monolayer MoS<sub>2</sub> photoluminescence intensity after annealing at different temperatures for 30 min. The PL intensity is optimally enhanced after annealing at 450°C.

The striking difference in the gas sensitivity in annealed and un-annealed (as-exfoliated) monolayer TMDs suggests two possibilities. First, a contamination layer might be present on the as-exfoliated surface, preventing O<sub>2</sub> or H<sub>2</sub>O molecules from interacting with the TMD surface. Organics and molecules are known to be easily adsorbed on chemically inert TMD surfaces [4, 5]. Thermal anneal at 450 °C might clean off this contamination layer, exposing and sensitizing the TMD surface to electronegative gas molecules. The second possibility is that the thermal anneal at 450°C creates a small density of chalcogen vacancies in the monolayer TMD, which facilitate the subsequent physisorption of O<sub>2</sub> and/or H<sub>2</sub>O molecules on the surface. To illustrate this point, we have taken Auger electron spectrum of pristine and annealed monolayer MoS<sub>2</sub> with 100 nm spot size (nano-Auger). Here, the monolayer MoS<sub>2</sub> was annealed *in-situ* for 30 min. As shown in Fig.S3, we observe that the annealing slightly reduces the S/Mo ratio, implying that chalcogen vacancies are created at small densities.

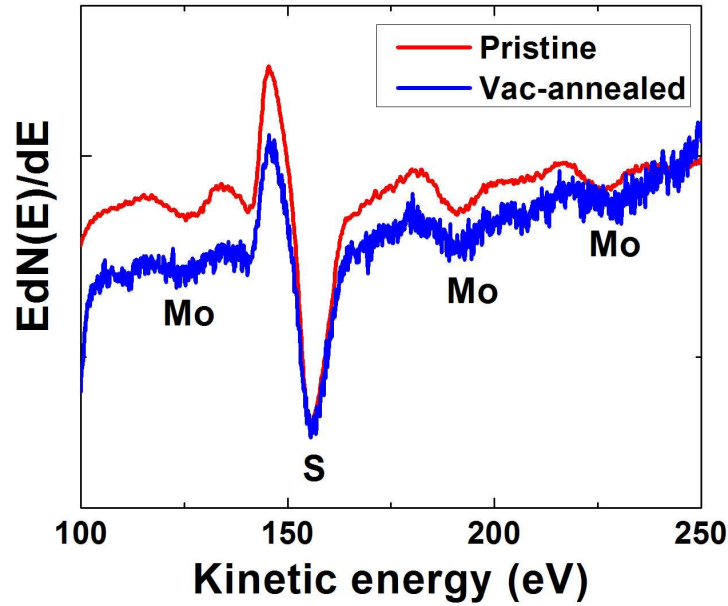


**Figure S3.** Nano-Auger electron spectroscopy data on pristine and annealing  $\text{MoS}_2$ . The S to Mo ratio is slightly reduced implying that small chalcogen vacancies are created. Here the intensity of each element is represented by the peak-to-valley height of the corresponding feature.

The Raman spectroscopy data provides very valuable information about the effect of thermal annealing on the monolayers. Following Fig. 1b inset, the in-plane ( $E_{2g}$ ) mode softens and the out-of-plane ( $A_g$ ) mode remains unchanged after the annealing process. Given these findings, if the contamination layer were to fully cover the surface, the out-of-plane mode would soften after this layer is thermally driven away. Instead,  $A_g$  remains unchanged implying that the residual layer may not fully cover the surface, which is consistent with our measured monolayer thickness (0.7 nm) using contact-mode AFM. Therefore, removal of the residual layer is not the sole reason for enhanced PL.

On the other hand, the softening in the  $E_{2g}$  mode implies that the monolayers are relaxed (softened) after the annealing, possibly due to: 1) releasing the strain that is induced by the substrate, 2) introducing a small density of defects as evidenced by the small increase in FWHM of  $E_{2g}$  peak, and 3) desorption of contamination on the monolayers.

### 3. Electrical gating in vacuum and in air

Our measurements in controlled gas environments and vacuum condition along with DFT calculations propose that the interaction between the gas molecules and  $\text{MX}_2$  monolayers is the most important factor determining the PL modulation. To test this hypothesis, we deplete a monolayer  $\text{MoS}_2$  by electrical field gating (Fig.S3) and simultaneously monitor the PL spectrum.

Surprisingly, a strong PL modulation by gating is observed only when the sample is in air, and the effect mostly disappears when the sample is measured in vacuum. This implies that the main gating effect still functions through the interaction between the molecules in air (more specifically,  $O_2$  and  $H_2O$ ) and the monolayer  $MoS_2$ . The electrical gating catalyses the interaction between the molecules and  $MoS_2$ , possibly by deepening the physisorption potential and enhancing the amount of charge transfer per molecule.

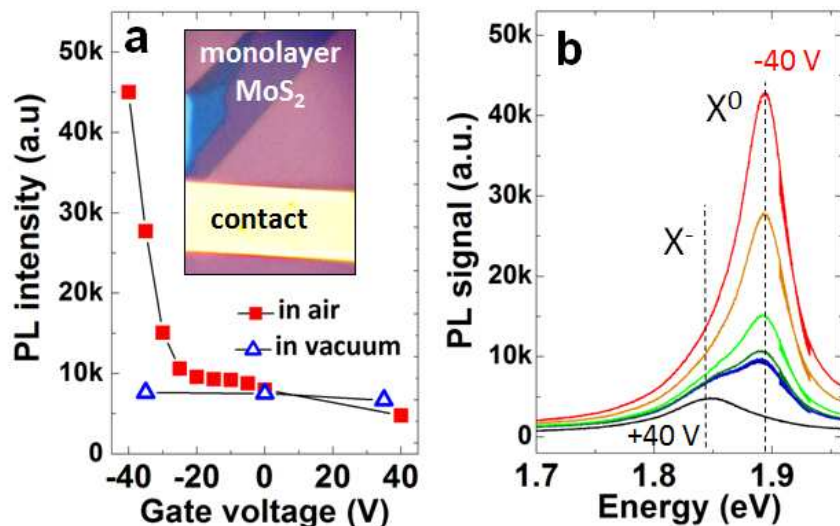


**Figure S4. Gate modulation of light emission in monolayer  $MoS_2$ .** *a.* PL intensity in accumulation (positive gate voltages) and depletion (negative gate voltages) modes measured in air and in vacuum conditions. Inset, top-view optical image of the device for electrical gating. *b.* PL signal measured as a function of gating voltage in air.

## References

- [1] Benameur, M.M. *et al.* Visibility of dichalcogenide nanolayers, *Nanotechnology* 22, 125706 (2011).
- [2] Lee, C. *et al.* Anomalous Lattice Vibrations of Single- and Few-Layer  $MoS_2$ . *ACS Nano*, 4, 2695 (2010).
- [3] Mak, K. F. *et al.* Atomically Thin  $MoS_2$ : A New Direct-Gap Semiconductor. *Phys. Rev. Lett.* 105, 136805 (2010); Mak, K. F. *et al.* Control of valley polarization in monolayer  $MoS_2$  by optical helicity. *Nature Nanotech.* 7, 494 (2012)
- [4] Hara, M. *et al.* A. Anchoring structure of smectic liquid-crystal layers on  $MoS_2$  observed by scanning tunnelling microscopy. *Nature*, 344, 228 (1990).
- [5] Qiu, H., *et al.* Electrical characterization of back-gated bi-layer  $MoS_2$  field-effect transistors and the effect of ambient on their performances. *Appl. Phys. Lett.*, 100, 123104 (2012).